Robotica (1997) volume 15, pp 319–329. Printed in the United Kingdom © 1997 Cambridge University Press

Task space dynamic analysis for multi-arm robot using isotropic velocity and acceleration radii

Choong-Young Kim and Yong-San Yoon

Department of Mechanical Engineering, Korea Advanced Institute of Science and Technology, 373-1 Kusung-dong, Yusung-Gu, Taejon, 305-701 (Korea)

(Received in final form: July 16, 1996)

SUMMARY

Isotropic velocity radius (*IVR*) and isotropic acceleration radius (*IAR*) are proposed as local performance indices to quantify the dynamic responsiveness of a multi-arm robot as regards the velocity effects. These performance measures are defined on the basis of the acceleration set describing the effects of actuator torques, velocity of the manipulated object, and gravity upon the acceleration of the object. An algorithm is presented to obtain an explicit expression for calculating these measures by decomposing the torque-related non-square matrix into square matrices without using the concept of pseudo-inverse for the planar multi-arm robot composed of arms each with two joints.

Numerical examples for a planar robot with two 2R arms show that the proposed concepts are effective in representing the acceleration capability and velocity effects of a multi-arm robot.

KEYWORDS: Task space formulation; Multi-arm robot; Acceleration set: Isotropic acceleration radius; Isotropic velocity radius.

1. INTRODUCTION

Recently there is an increasing interest in robot systems with multiple arms to execute a certain task cooperatively. One may expect that such system could efficiently perform many applications which are impossible otherwise. Expected applications include tasks, such as manipulation of heavy, voluminous, or non rigid objects, assembly or manipulation of mechanical parts without the aid of fixtures or jigs, and space robotics applications. However, such systems are complex due to interactions among arms and we cannot directly use many well-known results from a single arm robot study.

For improved design and operation of a manipulator, it is important for the designer and operator to understand the characteristics of the manipulator such as dynamic responsiveness (speed and acceleration capability). Although it is difficult to characterize complex manipulator dynamics by a simple index because of complicated behavior including varying inertia, nonlinearity of Coriolis and centrifugal forces, and interactions among joints, several researchers have developed indices for a single arm manipulator. The generalized inertia ellipsoid (GIE) was proposed by Asada[1] to represent the capability of an end-effector's velocity. Yoshikawa[2] proposed a manipulability ellipsoid as a measure of ease of changing the end-effector's configuration by a set of joint velocities. The acceleration capability of a manipulator plays also an important role in determining its dynamics performance. Yoshikawa[3] proposed dynamic manipulability and dynamic manipulability ellipsoids which are essentially based on linear mapping between the acceleration of the end-effector and the joint torques without taking into account the nonlinearities from joint velocities. For representing the acceleration and velocity capability, Thomas et al[4] introduced minimum upper bounds of the magnitudes of the end-effector's acceleration and velocity with which the manipulator can overcome the inertia forces induced. For a 2-dof planar robot, Graettinger and Krogh[5] introduced an acceleration radius as a global performance measure. The acceleration radius represents an uniform lower bound on the magnitude of the end-effector's acceleration for any state of a joint position and velocity over the entire operating region. However, it needs extensive calculations and will generally be zero unless the operating region is small enough. Kim[6] analytically developed a theory of the acceleration sets for 2-dof planar and 3-dof spatial manipulators and defined several useful acceleration-based local performance measures: Maximum possible accelerations and isotropic accelerations at rest and in motion, respectively. Kim and Yoon[7] suggested a moving acceleration radius representing the isotropic acceleration for a 3-dof planar redundant robot.

But there are only a few measures suggested for the multi-arm robot. Lee[8] defined the dual-arm manipulability by the volume of intersection between two manipulability ellipsoids from individual arms. Chiacchio et al[9] extended the force and velocity ellipsoids defined by Yoshikawa to a multi-arm robot system. They[10] also defined dynamic manipulability ellipsoid of a multi-arm robot system. But the measure cannot represent the complete acceleration capability for a manipulated object because the system equations are approximate using the pseudo-inverse concept.

Our study is intended to provide some useful tools for an analytical and graphical representation of the dynamic responsiveness of multi-arm robots. At higher speeds the effect of velocity terms becomes more important. Two measures, isotropic acceleration and velocity radii, are proposed to characterize the dynamic performance taking into account the velocity effect. For that

https://doi.org/10.1017/S0263574797000362 Published online by Cambridge University Press

purpose, an accleration set for multi-arm robots is selected to describe the effects of actuator torques, velocity of the manipulated object, and gravity upon on the acceleration of the object. We also developed an algorithm to obtain some concise explicit expressions for isotropic acceleration and velocity radii without using pseudo-inverse.

In Section 2, we are considering a multi-arm manipulator with an object in rigid contact and deriving dynamic equations completely in the task space. From these equations, we can obtain three fundamental mappings from the actuator torques, velocity of the object, and gravity to the acceleration of the object respectively. Using these mappings, the acceleration sets are determined in Section 3. Section 4 illustrates the concepts of isotropic acceleration and velocity radii. It also shows an algorithm to obtain explicit expressions for the measures by the decomposition of non-square torque-related matrices into squre ones. In Section 5, we are taking a planar robot with two 2R arms as an example to show the validity of the proposed approach.

2. TASK SPACE DYNAMIC MODELING OF MULTI-ARM ROBOTS

In this section, we formulate system equations to completely relate the absolute accelerations achievable by the manipulated object with the actuator torques of each arm, gravity and the velocity terms. The joint space dynamic models have been the bases for various approaches to dynamic control of manipulators. However, to analyze and control the motion of the end effector and object, task space models are preferred. First, we derive the dynamics of the object and arms in the task space. Then the equations are assembled to construct the integrated system equations. The system under consideration consists of the manipulated object and L number of arms cooperatively holding it (Figure 1). We assume that the object is rigid and tightly grasped by the end-effectors.

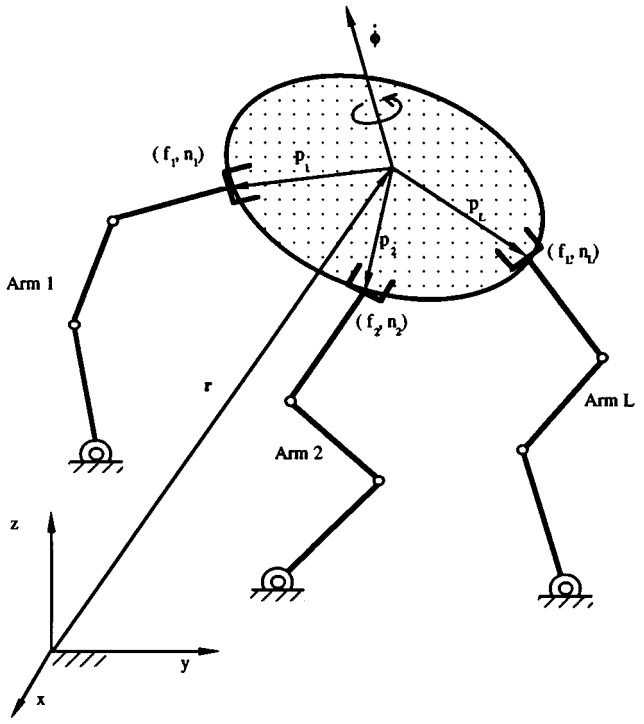


Fig. 1. Multi-arm robot cooperatively holding an object.

2.1 Dynamics of manipulated object

Let $F_c = [f_c^T n_c^T]^T \in R^m$ be the resultant force and moment vectors applied at the center of mass of the object and $F_i = [f_i^T n_i^T]^T \in R^m$, $i = 1, \ldots, L$ be the reaction force and moment vectors exerted by i-th robot arm to the object. the resultant force and moment have the relations

$$f_c = \sum_{i=1}^{L} f_i + m_c g \tag{1}$$

and

$$n_c = \sum_{i=1}^{L} (p_i \times f_i + n_i) \tag{2}$$

where m_c is the mass of the object and p_i is the position vector of i-th contact point. These[11] can be also written in the matrix form as

$$F_c = WF + G_c \tag{3}$$

where

$$F = [F_1^T \cdots F_L^T]^T \in R^{mL}$$

$$W = [W_1 \cdots W_L] \in R^{m \times mL}$$

$$W_i = \begin{bmatrix} I & 0 \\ S_i & I \end{bmatrix} \in R^{m \times m}$$

$$S_i = \begin{bmatrix} 0 & -p_{iz} & p_{iy} \\ p_{iz} & 0 & -p_{ix} \\ -p_{iy} & p_{ix} & 0 \end{bmatrix} \quad \text{if } P_i = (p_{ix}, p_{iy}, p_{iz}) \in R^3$$

$$G_c = \begin{bmatrix} m_c g \\ 0 \end{bmatrix} \in R^m$$

Let $X = [r^T \ \phi^T]^T \in R^m$ be the position vector of the mass center of the object with respect to the world coordinate. then the equations of motion of the object are represented by the following Newton–Euler equations:

$$f_c = m_c \ddot{r} \tag{4}$$

$$n_c = I\ddot{\phi} + \dot{\phi} \times I\dot{\phi} \tag{5}$$

where I is the moment of inertia. These can be rewritten in a matrix form as

$$F_c = M_c(X)\ddot{X} + H_c(X, \dot{X}) \tag{6}$$

where

$$M(X_c) = \begin{bmatrix} m_c E & 0 \\ 0 & I \end{bmatrix} \in R^{m \times m}$$

$$H_c(X, \dot{X}) = \begin{bmatrix} 0 \\ \dot{\phi} \times I\dot{\phi} \end{bmatrix} \in R^m$$

and E is an identity matrix. Here each component of

https://doi.org/10.1017/S0263574797000362 Published online by Cambridge University Press

$H_c(X, \dot{X})$ is a quadratic function of $\dot{X}$ and can be expressed as

$$H_{cj}(X, \dot{X}) = \dot{X}^T \hat{H}_{cj}(X)\dot{X}, \quad j = 1, \ldots, m \tag{7}$$

Finally equations (3) and (6) are combined to produce that

$$WF = M_c(X)\ddot{X} + H_c(X, \dot{X}) - G_c \tag{8}$$

2.2 Dynamics of arm

The equations of motion of each arm without carrying object are given by

$$\tau_i = D_i(q_i)\ddot{q}_i + V_i(q_i, \dot{q}_i) + G_i(q_i) \tag{9}$$

where $q_i \in R^m$, $i = 1, \ldots, L$ denote the vector of joint variables of i-th arm, $D_i(q_i)$ is $m \times m$ inertia matrix, $V_i(q_i, \dot{q}_i)$ is a vector containing Coriolis and centrifugal acceleration terms, $G_i(q_i)$ is a vector of gravity terms, and τ_i is a joint torque vector of i-th arm. Here, all vectors have the dimension of m.

In order to take into account the reaction forces and moments due to the object, we consider the relations between the object position vector X and i-th arm joint variable q_i as follows:

$$X = \Psi_i(q_i) \tag{10}$$

$$\dot{X} = J_i(q_i)\dot{q}_i \tag{11}$$

$$\ddot{X} = J_i(q_i)\ddot{q}_i + \dot{J}_i(q_i)\dot{q}_i \tag{12}$$

where $$J_i(q_i) = \frac{\partial \Psi_i(q_i)}{\partial q_i} \in R^{m \times m}.$$

The equations of motion of i-th arm are given by

$$\tau_i = D_i(q_i)\ddot{q}_i + V_i(q_i, \dot{q}_i) + G_i(q_i) + J_i^T(q_i)W_iF_i \tag{13}$$

We can use equations (10), (11), and (12) to rewrite equation (13) with respect to the world coordinate. Firstly equation (13) can be changed using equation (12) as follows:

$$\begin{aligned}\tau_i = {} & D_i J_i^{-T}\ddot{X} + V_i(q_i, \dot{q}_i) - D_i J_i^{-T}\dot{J}_i\dot{q}_i \\ & + G_i(q_i) + J_i^T(q_i)W_iF_i\end{aligned} \tag{14}$$

Here each component of $V_i(q_i, \dot{q}_i) - D_i J_i^{-T}\dot{J}_i\dot{q}_i$ is a quadratic function of $\dot{q}_i$ and can be written in the form,

$$V_i(q_i, \dot{q}_i) - D_i J_i^{-T}\dot{J}_i\dot{q}_i = H_i(X, \dot{X}) \tag{15}$$

where $H_i(X, \dot{X})$ is a vector whose j-th component is

$$H_{ij}(X, \dot{X}) = \dot{q}_i^T U_j(q_i)\dot{q}_i = \dot{X}^T J_i^{-T} U_j J_i^T \dot{X} = \dot{X}^T \hat{H}_{ij}(X)\dot{X}$$

Therefore the dynamic equations[12] of i-th arm can be expressed in the world coordinate as

$$\tau_i = M_i(X)\ddot{X} + H_i(X, \dot{X}) + G_i(X) + J_i^T(q_i)W_iF_i \tag{16}$$

where

$$M_i(X) = D_i J_i^{-T} \in R^{m \times m}$$

$$H_i(X, \dot{X}) = \begin{bmatrix} \dot{X}^T \hat{H}_{i1}(X)\dot{X} \\ \vdots \\ \dot{X}^T \hat{H}_{im}(X)\dot{X} \end{bmatrix} \in R^m$$

$$\hat{H}_{ij}(X) \in R^{m \times m}$$

2.3 Dynamics of integrated system

Now we derive the dynamic equations treating the multiple arms and object as one integrated system. From equations (8) and (16), we can obtain that

$$\begin{aligned} & M_c(X)\ddot{X} + H_c(X, \dot{X}) - G_c \\ & = \sum_{i=1}^{L} W_iF_i \\ & = \sum_{i=1}^{L} J_i^{-T}(\tau_i - M_i(X)\ddot{X} - H_i(X, \dot{X}) - G_i(X)) \end{aligned} \tag{17}$$

Let's introduce some variables such as

$$A'(X) = [J_1^{-T} \cdots J_L^{-T}] \in R^{m \times mL} \tag{18}$$

$$\tau = [\tau_1^T \cdots \tau_L^T]^T \in R^{mL} \tag{19}$$

$$I'(X) = \sum_{i=1}^{L} J_i^{-T} M_i + M_c \in R^{m \times m} \tag{20}$$

$$Q'(X, \dot{X}) = \begin{bmatrix} \dot{X}^T \hat{Q}_1'(X)\dot{X} \\ \vdots \\ \dot{X}^T \hat{Q}_m'(X)\dot{X} \end{bmatrix} = \sum_{i=1}^{L} J_i^{-T} H_i + H_c = R^m \tag{21}$$

$$R'(X) = \sum_{i=1}^{L} J_i^{-T} G_i - G_c \tag{22}$$

Then, equation (17) can be concisely rewritten as

$$A'(X)\tau = I'(X)\ddot{X} + Q'(X, \dot{X}) + R'(X) \tag{23}$$

By premultiplying $I'^{-1}(X)$, this becomes

$$A(X)\tau = \ddot{X} + Q(X, \dot{X}) + R(X) \tag{24}$$

where

$$A(X) = I'^{-1}A' \in R^{m \times mL}$$

$$Q(X, \dot{X}) = I'^{-1}Q' \in R^m$$

$$R(X) = I'^{-1}R' \in R^m$$

Note that the equation is represented in the $\ddot{X}$ space. Thus, $A(X)\tau$, $Q(X, \dot{X})$, and $R(X)$ show the effects of the actuator torques, velocities of the object, and the gravity upon the acceleration of the object respectively at a given configuration. The three terms in the equation provide three fundamental mappings: linear, quadratic and constant mappings. Unlike a single arm robot system, the matrix $A(X) \in R^{m \times mL}$ is non-square and the mobility of the system is less than the total number of the actuators in it. Thus the inverse dynamics problem cannot be solved uniquely, which renders many useful methods developed for a single arm arobot unusable.

https://doi.org/10.1017/S0263574797000362 Published online by Cambridge University Press

3. ACCELERATION SETS

In the following, we define acceleration sets to effectively analyze and visualize the dynamic characteristics of each term in equation (24).

3.1 Acceleration set due to torque

Let's denote $A(X)\tau$ as $\ddot{X}_\tau$ which represents the object acceleration due to actuator torques. It is called generalized acceleration due to torque. It is a linear, configuration-dependent mapping between the actuator torques and its generalized acceleration. Before determining the acceleration set, we may define the set of available actuator torques. We assume the robot arms have joint driving torque limits,

$$-\tau_{ij\,\max} \le \tau_{ij} \le \tau_{ij\,\max}, \quad j = 1, \ldots, m, \quad i = 1, \ldots, L \tag{25}$$

where $\tau_{ij\,\max}$ is the limit of τ_{ij}. The set of allowable actuator torques is defined as

$$T = \{\tau \,|\, |\tau_{ij}| \le \tau_{ij\,\max}, j = 1, \ldots, m, i = 1, \ldots, L\} \tag{26}$$

which constructs an mL-dimensional rectangular parallelepiped. Then the acceleration set due to the actuator torques can be obtained as

$$S_\tau = \{\ddot{X}_\tau \,|\, \ddot{X}_\tau = A\tau,\ \tau \in T\} \tag{27}$$

This represents the set of acceleration achievable by the actuators when there is neither velocity nor gravity. The acceleration set S_τ is clearly the image of T under the linear mapping $A(X)$ forming a polyhedron in the $\ddot{X}$ space.

There are some methods of calculating the image set S_τ. In the case of a single arm non-redundant robot, $A(X)$ is square and S_τ can be easily obtained by well-known properties of linear mapping; It becomes an m-dimensional parallelepiped (parallelogram when $m = 2$). For a planar redundant manipulator, with m greater than 2, $A \in R^{2\times m}$ is non square. Kim[7] proposed a theorem to determine the image set of the planar redundant robot: The range of the image set for the given configuration is a convex polygon with $2m$ edges in x-y plane and the components of τ at two vertices on an edge are all same but one component. Li et al[13] obtained the image set of multi-arm robot with method similar to Kim's. But this method is limited to 2-dimensional case and does not provide information about boundary surfaces of the image set which is important for calculating measures.

Now, we are proposing a more useful method for obtaining the image set for the planar case of $m = 2$. As the dimension of A is $2 \times L$, this can be divided into L square matrices,

$$A = [A_1 \cdots A_L], \quad A_i \in R^{2\times 2} \tag{28}$$

and

$$A\tau = \sum_{i=1}^{L} A_i\tau_i = A_1\tau_1 + \cdots + A_L\tau_L \tag{29}$$

There is a 1-1 correspondence between these terms and arms. The set of allowable torques of each arm is a rectangle and the image of torque set is a parallelogram. Summing these image sets, the acceleration set S_τ due to the actuator torques can be obtained as a polygon with $2 \times L$ parallel pairs of boundary sides. There is also 1-1 correspondence between the pairs of sides of S_τ and the actuators of arms.

To illustrate the procedure of obtaining the set S_τ, let's consider the following examples: The first example is the case when $L = 2$ and $m = 2$ (Figure 2a) with

$$\ddot{X}_\tau = A\tau = A_1\tau_1 + A_2\tau_2 \tag{30}$$

where

$$A = [A_1 \quad A_2] \in R^{2\times 4}, \quad A_i \in R^{2\times 2}$$
$$\tau = [\tau_1 \quad \tau_2]^T \in R^4, \quad \tau_i \in R^2$$

The set of the allowable torques of each arm is rectangular with 2 parallel pairs of sides. These pairs of sides correspond to the actuator torques of each arm: Side S_{ij} to j-th joint of i-th arm. The image of the torque set is a parallelogram and has also 2 parallel pairs of sides. Here, the pair S'_{ij} corresponds to S_{ij} of torque set. The acceleration set S_τ can be completed by fixing one parallelogram with its origin located at the origin of $\ddot{X}$ space and moving the origin of the other one everywhere within the fixed parallelogram. This procedure produces an octagon with 4 parallel pairs of sides as shown in Figure 2a. Each side S''_{ij} of the octagon corresponds to each S'_{ij} of the image of the torque set.

The second example is the case of $L = 3$ and $m = 2$ (Figure 2b) with

$$\ddot{X}_\tau = A\tau = A_1\tau_1 + A_2\tau_2 + A_3\tau_3 \tag{31}$$

where

$$A = [A_1 \quad A_2 \quad A_3] \in R^{2\times 6}, \quad A_i \in R^{2\times 2}$$
$$\tau = [\tau_1 \quad \tau_2 \quad \tau_3]^T \in R^6, \quad \tau_i \in R^2$$

From the previous results, we can see that the sum of first two terms produces an octagon and last term a parallelogram. Similarly the image set S_τ can be completed by fixing the octagon and moving the parallelogram within the fixed octagon. This procedure produces a dodecagon as shown in Figure 2b. Each side S''_{ij} of the dodecagon also has an 1-1 correspondence with S_{ij}.

The third example is the case of a 3-dof planar redundant robot with

$$A\tau = [A_1 \quad A_2 \quad A_3]\begin{Bmatrix}\tau_1\\ \tau_2\\ \tau_3\end{Bmatrix} \tag{32}$$

where

$$A = [A_1 \quad A_2 \quad A_3] \in R^{2\times 3}, \quad A_i \in R^2$$
$$\tau = [\tau_1 \quad \tau_2 \quad \tau_3]^T \in R^3, \quad \tau_i \in R^1$$

The matrix A can be divided into a 2×2 square matrix

https://doi.org/10.1017/S0263574797000362 Published online by Cambridge University Press

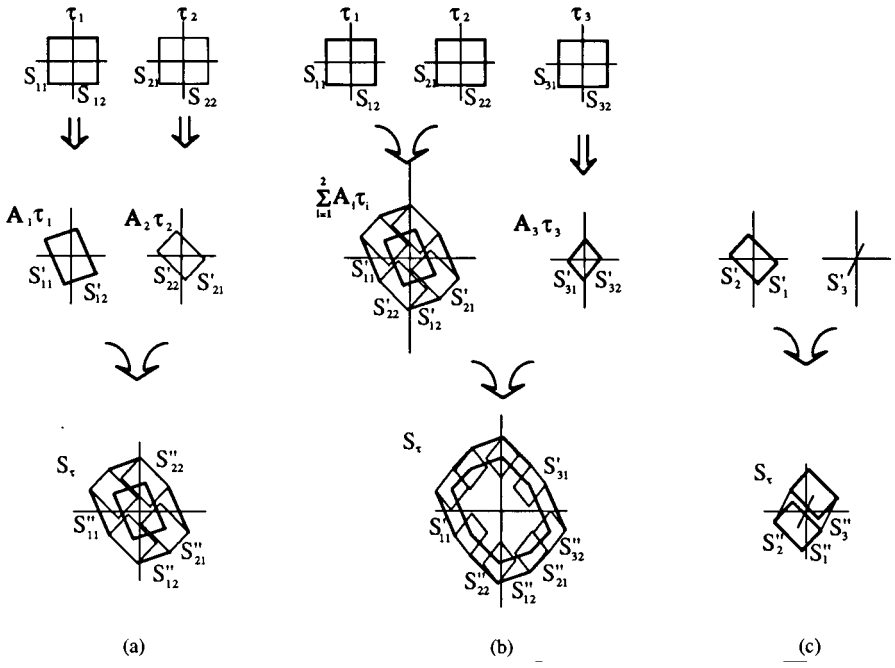


Fig. 2. Acceleration set due to actuator torques: (a) $L = 2$, $m = 2$ (b) $L = 3$, $m = 2$ (c) 3 dof planar redundant robot.

and a 2×1 non-square one in a various way. One of the partitions is

$$A\tau = [A_I \quad A_2]\left\{\frac{\tau_1}{\tau_2}\right\} + [A_3]\{\tau_3\} \tag{33}$$

Here, the first term is represented as a parallelogram and the second term is represented as a line. Figure 2c shows the combined acceleration set of the redundant robot.

3.2 Acceleration set due to velocity

The effect of object velocity on the object acceleration is represented by

$$Q(X, \dot{X}) = \begin{bmatrix} \dot{X}^T \hat{Q}_1(X)\dot{X} \\ \vdots \\ \dot{X}^T \hat{Q}_m(X)\dot{X} \end{bmatrix} \in R^m \tag{34}$$

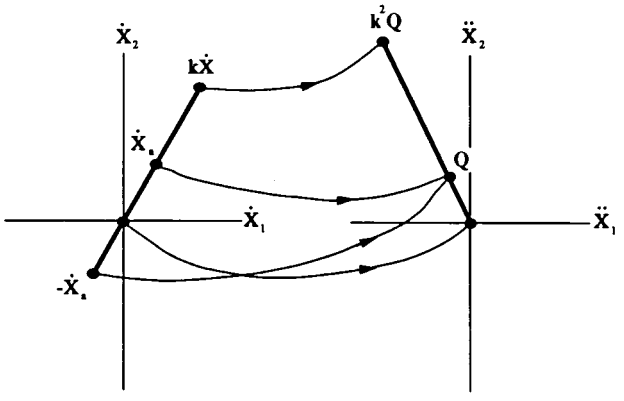


Fig. 3. Properties of quadratic mapping.

There is a quadratic, configuration-dependent mapping between the velocity of the object and the generalized acceleration due to it. This effect is complicated because it is a quadratic function of the velocity. Some fundamental properties of this quadratic mapping, as shown in Figure 3, are as follows:

(i) The origin of the $\dot{X}$-space maps into the origin of the $\ddot{X}$-space.
(ii) The direction of the object velocity is altered in its image on the $\ddot{X}$-space.
(iii) Two distinct points $\dot{X}$ and $-\dot{X}$ which are axi-symmetric with respect to the origin map into the same point in the $\ddot{X}$-space.
(iv) The function $Q(X, \dot{X})$ is proportional to the square of $\dot{X}$: For example, when $\dot{X}$ maps into $Q(X, \dot{X})$, $\kappa\dot{X}$ maps into $\kappa^2 Q(X, \dot{X})$. As the velocity increases, its effect increases quadratically.
(v) A straight line in the $\dot{X}$-space generally doesn't map into a straight line. However, a straight line with endpoints $\dot{X}$ and $-\dot{X}$ in the $\dot{X}$-space maps into a straight line with one endpoint at the origin and the other endpoint at $Q(X, \dot{X})$ in the $\ddot{X}$-space.

In order to visualize the effect of the object velocity, let's consider the object moving with speed v in a direction. These motions are represented by the set,

$$V = \{\dot{X} | \, \|\dot{X}\| = v\} \tag{35}$$

The acceleration set due to these motions becomes an ellipsoid,

$$S_v = \left\{ Q \,\middle|\, Q(X, \dot{X}) = \begin{bmatrix} \dot{X}^T \hat{Q}_1(X)\dot{X} \\ \vdots \\ \dot{X}^T \hat{Q}_m(X)\dot{X} \end{bmatrix}, \dot{X} \in V \right\}. \tag{36}$$

https://doi.org/10.1017/S0263574797000362 Published online by Cambridge University Press

The center of the ellipsoid is

$$\left(\frac{v^2}{2}((\lambda_1)_{\min}+(\lambda_1)_{\max}),\ldots,\frac{v^2}{2}((\lambda_m)_{\min}+(\lambda_m)_{\max})\right) \quad (37)$$

The center varies in proportion to the square of the velocity and the ellipsoid may not include the origin of the $\ddot{X}$-space as shown in Figure 4. The minimum and maximum values of i-th component of the image set $Q(X, \dot{X})$ are, respectively, $v^2(\lambda_i)_{\min}$ and $v^2(\lambda_i)_{\max}$ where λ_i are the eigenvalues of the quadratic matrix $\hat{Q}_i(X)$. From the ellipsoid, we can identify the magnitude and direction of the effect of object velocity. The longer the distance between the origin and the points on the ellipsoid in the $\ddot{X}$-space is, the larger the effect of object velocity is and the poorer the acceleration capability in that direction is.

3.3 Acceleration set due to gravity

The effect of gravity on the object acceleration is represented by the vector $R(X)$ and is only configuration dependent.

4. ISOTROPIC ACCELERATION AND VELOCITY RADII OF MULTI-ARM ROBOTS

4.1 Definitions

In the previous section, the acceleration set has been presented as a tool to analyze and visualize the dynamics of a multi-arm robot. In the case where the object velocity is zero, the acceleration capability can be obtained using the method suggested in Section 3.1 and is shown in Figure 5a. However, in motion, the acceleration capability will be shifted by $b = -Q(X, \dot{X}) - R(X)$ due to the object velocity in equation (24). This is depicted in Figure 5b. The magnitude and direction of the shifted value vary with those of the velocity, which is difficult to represent. In the single arm robot, some researchers expressed the robot dynamic performance only by the acceleration capability ignoring the velocity effects; this is insufficient for measuring the dynamic responsiveness of the robot. As the velocity effects grow quadratically, the effects become more prominent in at higher speeds. In this section, two

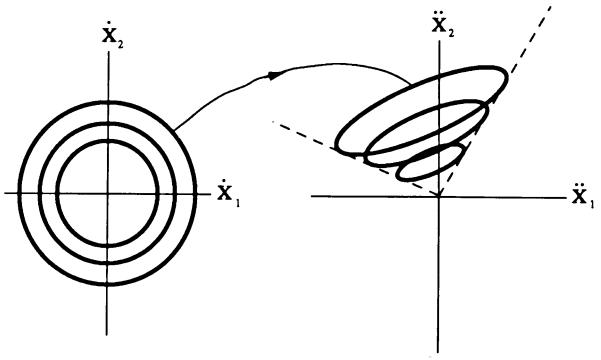


Fig. 4. Object motions with $\|\dot{X}\| = \text{const}$ and their quadratic mappings.

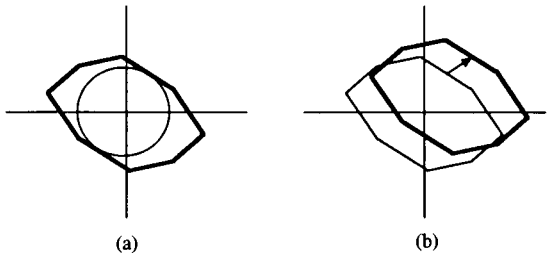


Fig. 5. Shift of acceleration set due to torques because of object velocity.

measures, isotropic acceleration radius (*IAR*) and isotropic velocity radius (*IVR*), are proposed to separate the acceleration effect and velocity effects in equation (24). *IAR* is the smallest magnitude among the maximum tip accelerations the actuators may produce in each direction (translation and rotation) at a given standing configuration. *IVR* is the smallest among the maximum tip velocity whose inertia forces the actuators may overcome in each direction at a given configuration with zero tip acceleration and gravity. In a single arm robot, Thomas et al[4] used these measures to simply represent the limits on the end-effector acceleration and velocity. However, the inverse dynamics problem cannot be solved uniquely in the multi-arm robot in contrast to the case of the single arm robot, which makes the algorithm developed for a single arm robot to be hardly applicable to a multi-arm robot.

We are proposing an algorithm to obtain compact and explicit expressions for determining *IAR* and *IVR* for a planar multi-arm robot. In a multi-arm robot, although an unique torque solution doesn't exist, the motions achievable under the given torques and the loads are uniquely determined in the acceleration space by equation (24). For the robot to accomplish a desired motion, the actuators must provide a generalized acceleration set due to the movements: If the generalized acceleration due to a desired motion is within the acceleration set due to torque, the motion is possible.

*4.2 Calculation of **IAR***

When $\dot{X} = 0$, equation (24) may be reduced to

$$A(X)\tau = \ddot{X} + R(X) \quad (38)$$

To calculate *IAR*, consider the motions having $\|\ddot{X}\| = \text{const}$. These motion under gravity are represented by an ellipsoid with center at $R(X)$. The larger the magnitude of the acceleration is, the larger the ellipsoid becomes. As previously stated, the acceleration set due to torque is a polyhedron for the general case and a polygon for the case of $m = 2$. *IAR* is the magnitude of the acceleration when the ellipsoid begins to touch the polygon. As there are $2 \times L$ symmetric pairs of sides in the polygon, *IAR* corresponds to the smallest among the accelerations with the ellipsoids tangent to the sides of the polygon. In a 2-dimensional case, we can directly calculate the value from distances between the center of the ellipsoid and the sides of the polygon. But this method can't be applicable directly to a general case.

https://doi.org/10.1017/S0263574797000362 Published online by Cambridge University Press

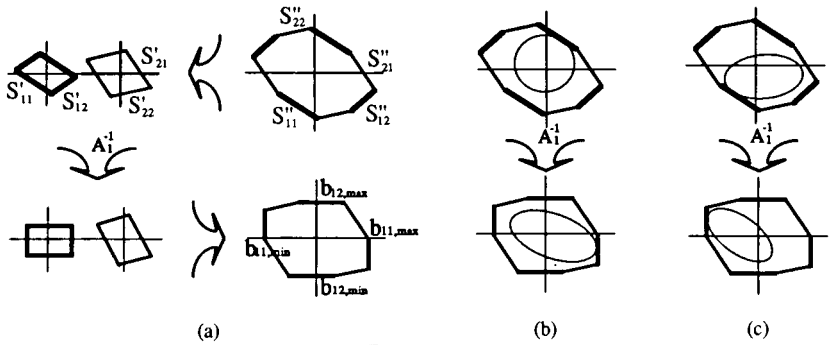


Fig. 6. (a) Decomposition and A_1^{-1} transformation of acceleration sets due to torques, and A_i^{-1} transformation of acceleration sets due to object motions with (b) $\|\dot{X}\| = \text{const}$ and (c) $\|\dot{X}\| = \text{const}$.

Let's calculate the magnitude of the acceleration when the ellipsoid is tangent to S_{ij}'' sides of the polygon. The decomposition of $A\tau$ by equation (29) is shown in Figure 6a. By the transformation A_i^{-1}, equation (37) becomes

$$\tau_i + \sum_{k \neq i}^{L} A_i^{-1} A_k \tau_k = A_i^{-1} \ddot{X} + A_i^{-1} R \tag{39}$$

Ths sides S_{ij}'', $j = 1, 2$ of the polygon corresponding to i-th arm is normal to the axes of m-dimensional space and the ellipsoid remains tangent to the side by the properties of the linear transformation (Figure 6b). The maximum value of each component of the vector $A_i^{-1} A_k \tau_k$ is

$$\max (A_i^{-1} A_k \tau_k)_j = \sum_{l=1}^{2} |(A_i^{-1} \ A_k)_{jl}| \ \tau_{kl,\max}, \quad k = 1, \ldots, L, \quad k \neq i \tag{40}$$

where $|(A_i^{-1} \ A_k)_{jl}|$ is the absolute value of jl-element of the matrix $A_i^{-1} A_k$ and $\tau_{kl,\max}$ is the maximum torques of l-th actuator of k-th arm. So the maximum value of j-th component of the left side of equation (39) is

$$b_{ij,\max} = \sum_{k \neq i}^{L} \sum_{l=1}^{2} |(A_i^{-1} \ A_k)_{jl}| \ \tau_{kl,\max} + \tau_{ij,\max} \tag{41}$$

Similarly, the minimum value is (Figure 6a)

$$b_{ij,\min} = -b_{ij,\max} \tag{42}$$

These minimum and maximum values are j-th components of sides which S_{ij}'' is transformed into.

The problem of calculating the magnitude of acceleration of the ellipsoid tangent to S_{ij}'' can be stated as

$$\begin{aligned} &\text{Maximize } \|\ddot{X}\| \\ &\text{subject to } b_{ij,\min} \leq (A_i^{-1})_j \ddot{X} + (A_i^{-1})_j R \leq b_{ij,\max} \end{aligned} \tag{43}$$

where $(A_i^{-1})_j$ is j-th row of the matrix A_j^{-1}. The constraint equation can be changed as

$$b_{ij,\min} - (A_i^{-1})_j R \leq (A_i^{-1})_j \ddot{X} \leq b_{ij,\max} - (A_i^{-1})_j R \tag{44}$$

Using a weighted pseudo-inverse, the magnitude of the ellipsoid tangent to S_{ij}'' can be obtained as

$$IAR^{ij} = [(A_i^{-1})_j]^{\#} b_{ij,\text{ext}} \tag{45}$$

where $b_{ij,\text{ext}} = \min \{|b_{ij,\min} - (A_i^{-1})_j R|, |b_{ij,\max} - (A_i^{-1})_j R|\}$ and superscript # denotes the weighted pseudo-inverse. In this way, we can determine the magnitude of the acceleration for the ellipsoid tangent to the sides of the polygon. Finally IAR can be obtained as

$$IAR = \min \{IAR^{ij}, i = 1, \ldots, L, j = 1, 2\} \tag{46}$$

This method can be applicable to the redundant robot. For example, in the case of 3-dorf redundant robot, the acceleration set due to torque is given by equation (32) as shown in Figure 2c. Partitioning as in equation (33), IAR's corresponding to S_1'' and S_2'' can be obtained by $[A_1 \ A_2]^{-1}$ transformation. Similarly we may partition the matrix A as such that

$$A\tau = [A_1 \ A_3] \begin{Bmatrix} \tau_1 \\ \tau_3 \end{Bmatrix} + [A_2]\{\tau_2\} \tag{47}$$

Then IAR's corresponding to S_1'' and S_3'' can be obtained by $[A_1 \ A_3]^{-1}$ transformation.

4.3 Calculation of ***IVR***

The isotropic velocity radius represents only the velocity effects. Thus equation (24) may be reduced to

$$A(X)\tau = Q(X, \dot{X}) \tag{48}$$

This effect is rather difficult to handle and we want to limit our study to the case when $\|\dot{X}\| = \text{const}$. These velocity effects are represented by an ellipsoid. But the center of the ellipsoid depends on the object velocity and the eigenvalues of the quadratic matrices $\hat{Q}_i$, $i = 1, 2$. As the acceleration set due to torque is a polygon, IVR is the magnitude of the velocity when the ellipsoid is tangent to S_{ij}'' sides of the polygon. By the transformation A_i^{-1}, equation (48) becomes

$$\tau_i + \sum_{k \neq i}^{L} A_i^{-1} A_k \tau_k = A_i^{-1} Q \tag{49}$$

As before, the problem of determining the velocity

https://doi.org/10.1017/S0263574797000362 Published online by Cambridge University Press

when the ellipsoid is tangent to the polygon can be stated as

$$\begin{aligned} &\text{Maximize } \|\dot{X}\| \\ &\text{subject to } b_{ij,\min} \le (A_i^{-1})_j Q \le b_{ij,\max} \end{aligned} \tag{50}$$

As $(A_i^{-1})_j Q$ is a quadratic function of $\dot{X}$, the constraint equation can be rewritten as

$$b_{ij,\min} \le \dot{X}^T P_{ij}(X) \dot{X} \le b_{ij,\max} \tag{51}$$

where

$$(A_i^{-1})_j Q = \dot{X}^T P_{ij}(X) \dot{X}$$

Table I. Specification of planar 2 link robot constructing multi-arm robot.

	link 1	link 2
length (m)	0.303	0.303
center of mass [m]	0.196	0.088
mass [Kg]	2.259	1.126
moment of inetia [Kg m^2]	0.129	0.103
peak torque [Nm]	60	40

The magnitude of the velocity vector $\dot{X}$ is defined as

$$v = \|\dot{X}\| = (\dot{X}^T W_v \dot{X})^{1/2} \tag{52}$$

where W_v is a diagonal weighting matrix.

The object velocity can be expressed in terms of its unit vector e_v and magnitude v as

$$\dot{X} = v e_v \tag{53}$$

where

$$e_v^T W_v e_v = 1 \tag{54}$$

Then,

$$\dot{X}^T P_{ij} \dot{X} = v^2 e_v^T P_{ij} e_v = v^2 \frac{e_v^T P_{ij} e_v}{e_v^T W_v e_v} = v^2 \frac{e_v^T W_v^{-1} P_{ij} e_v}{e_v^T e_v} \tag{55}$$

The right-hand side of the equation is in the form of a Rayleigh quotient which results in the solution,

$$(\lambda_{ij})_{\min} \le \frac{e_v^T W_v^{-1} P_{ij} e_v}{e_v^T e_v} \le (\lambda_{ij})_{\max} \tag{56}$$

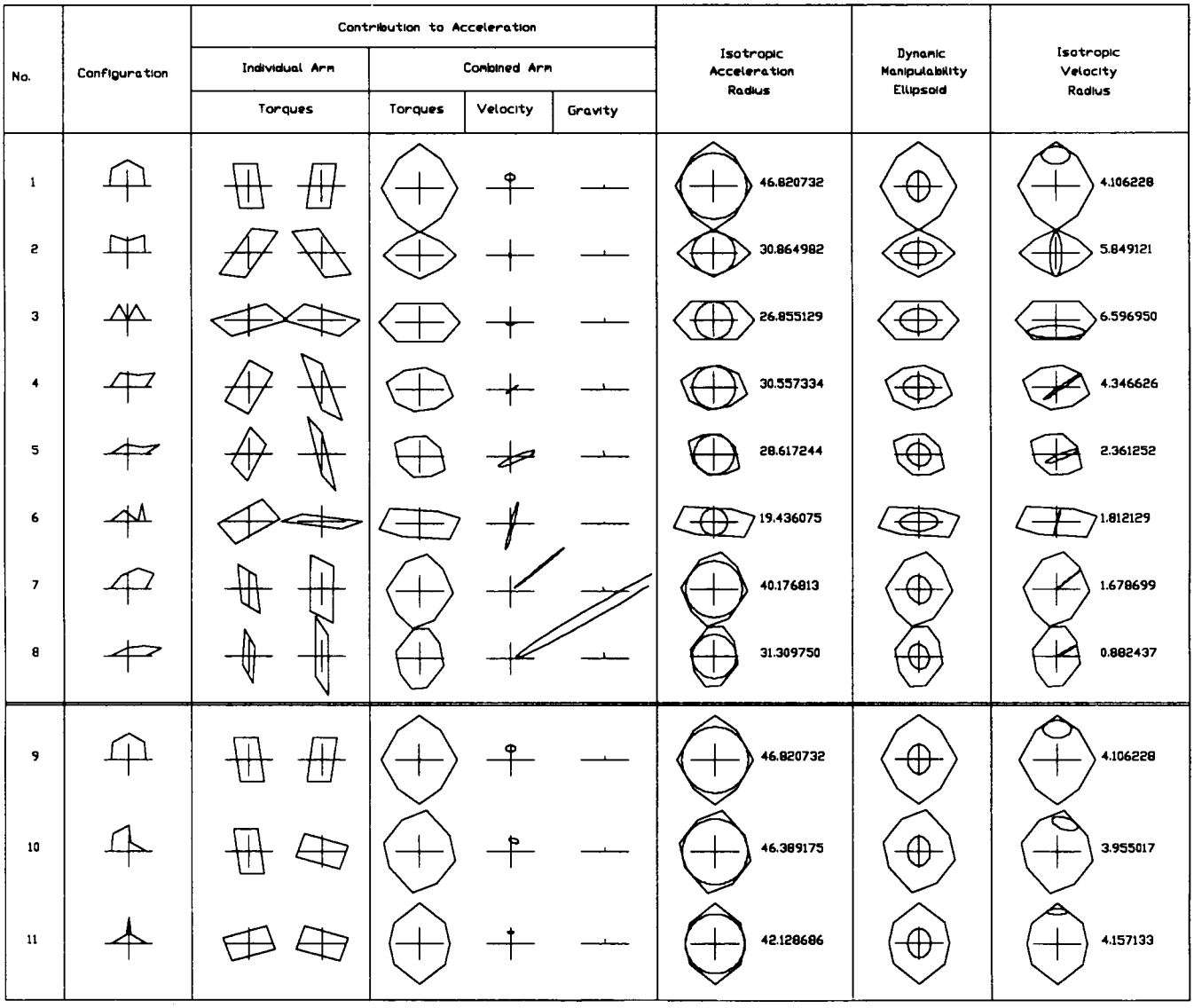


Fig. 7. Acceleration sets due to actuator torques in individual arm constructing multi-arm robot and acceleration sets due to actuator torques, object velocities, and gravity in multi-arm robot, and IAR, IVR and dynamic manipulability of multi-arm robot.

https://doi.org/10.1017/S0263574797000362 Published online by Cambridge University Press

where λ_{ij} are the eigenvalues of the symmetric matrix

$$\tfrac{1}{2}W_v^{-1}\{P_{ij} + P_{ij}^T\} \tag{57}$$

Therefore the ellipsoid should be in the range,

$$v^2(\lambda_{ij})_{\min} \le \dot{X}^T P_{ij} \dot{X} \le v^2(\lambda_{ij})_{\max} \tag{58}$$

From equations (51) and (58), the magnitude of the velocity of the ellipsoid tangent to S_{ij}'' of the polygon is determined as

$$IVR^{ij} = \begin{cases} \left\{\min\left\{\dfrac{b_{ij,\min}}{(\lambda_{ij})_{\min}}, \dfrac{b_{ij,\max}}{(\lambda_{ij})_{\max}}\right\}\right\}^{1/2}, & \text{if } (\lambda_{ij})_{\min}(\lambda_{ij})_{\max} < 0 \\ \left(\dfrac{b_{ij,\min}}{(\lambda_{ij})_{\min}}\right)^{1/2}, & (\lambda_{ij})_{\max} < 0 \\ \left(\dfrac{b_{ij,\max}}{(\lambda_{ij})_{\max}}\right)^{1/2}, & (\lambda_{ij})_{\min} > 0 \end{cases} \tag{59}$$

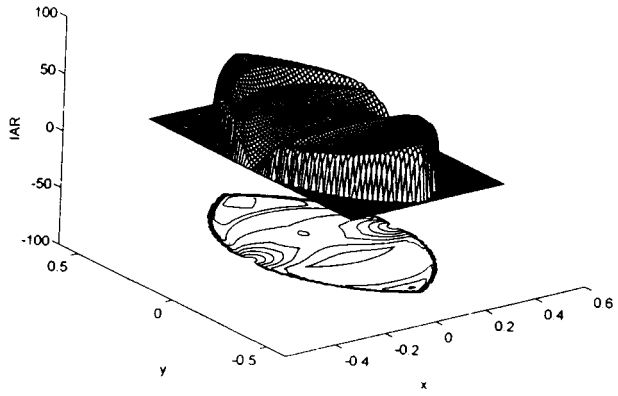
We can obtain *IVR* as

$$IVR = \min\{IVR^{ij},\ i = 1, \ldots, L,\ j = 1, 2\} \tag{60}$$

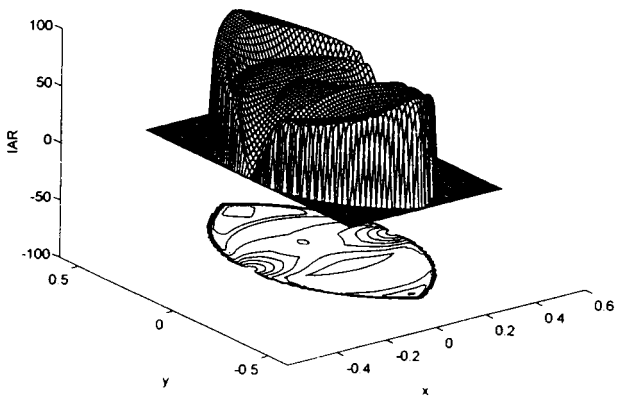
Now we may illustrate the analysis of robot dynamic performance with *IAR* and *IVR*. Generally, for the case when the object velocity is zero, the acceleration capability is shown in Figure 5a and can be approximately represented by *IAR*. However, in motion, the acceleration capability is shifted due to the velocity effect and the isotropic acceleration capability deteriorates accordingly. If the effect is more than a certain extent, the isotropic acceleration capability becomes zero. *IVR* is a measure of the velocity effect on the acceleration capability. If *IVR* is large, the velocity effect is small and the acceleration capability doesn't change much. For example, for the case when both of *IAR* and *IVR* are large, the acceleration capability at stationary state is good and deteriorates slowly according to the object velocity. If *IVR* is small, the acceleration capability is shifted largely and the isotropic acceleration capability deteriorates rapidly to zero as the object velocity increases.

5. RESULTS AND DISCUSSIONS

A planar robotic system composed of two arms each with two rotational joints[14] manipulating a common rigid body is taken as an example. Both arms have same specifications as shown in Table I and the object mass is

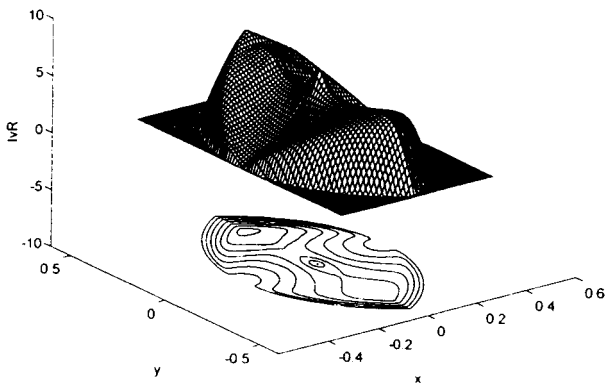


(a)

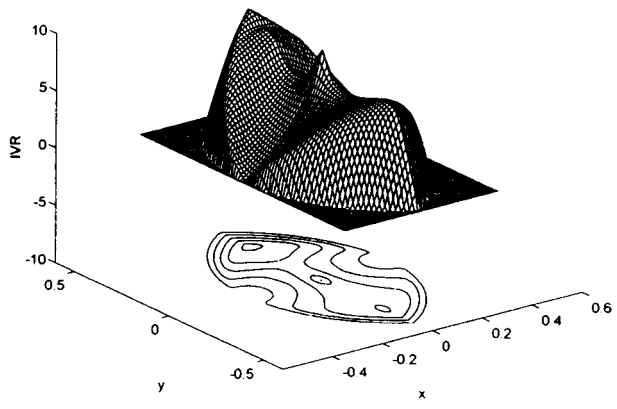


(b)

Fig. 8. *IAR* for (a) $\tau_1 = 60,\ \tau_2 = 40$ (b) $\tau_1 = 120,\ \tau_2 = 80$.



(a)



(b)

Fig. 9. *IVR* for (a) $\tau_1 = 60,\ \tau_2 = 40$ (b) $\tau_1 = 120,\ \tau_2 = 90$.

https://doi.org/10.1017/S0263574797000362 Published online by Cambridge University Press

6.0 kg. The distance between the center points of the bases of two arms is 0.6 m. All other quantities are referred to the inertial frame which is located at the middle of two bases.

5.1 Acceleration sets

The acceleration sets due to torque for individual arm and the acceleration sets due to torque, velocity and gravity for the multi-arm robot are depicted in Figure 7. The acceleration set due to torque for each arm is a quadrilateral, while that for the multi-arm robot is an octagon and more isotropic due to the constraints imposed by the cooperation than that for the single arm robot. This fact reveals that *IAR* is more useful to represent the acceleration capability for the multi-arm robot than the single arm robot. There are large variations in the acceleration sets due to the object motion as shown for the case when the velocity is $\|v\| = 2.5$ m/sec. In Cases 2 or 3, the velocity effect is very small and the acceleration capability doesn't change much as velocity increases. In Cases 7 or 8, the velocity effect is very large and the acceleration capability deteriorates rapidly as velocity increases. In Case 1, the velocity effect is in the upper side and the system in this state has difficulty in accelerating upwards. Similarly, in Cases 7 or 8, the system has difficulty in accelerating at 45 degree direction. On the other hand, there are little variations in the acceleration sets due to gravity.

5.2 ***IAR*** *and* ***IVR***

Figure 7 shows *IAR* and *IVR* for some configurations with no gravity. *IAR* more closely represents the acceleration capability for multi-arm robot than the dynamic manipulability[15,16] using pseudo-inverse. In Cases 2 or 3, the acceleration capability is not large but *IVR* is large because the velocity effects are small; The acceleration capability slowly deteriorates to zero according to velocity increase. On the contrary, in Case 7, *IAR* is large but *IVR* small, and the acceleration capability rapidly deteriorates to zero according to velocity increase. Cases 9, 10 and 11 in Figure 7 show that the measures depend on the configuration as well as the object position. Figures 8 and 9 show *IAR* and *IVR* calculated for all configurations in the workspace. There is no gravity effect but the figure is not symmetric. The reason is that even if the object positions are asymmetric, the configuraions aren't. As the object is near the boundary of workspace, *IAR* is large but *IVR* small. For the case when gravity is considered, *IAR* are smaller while *IVR* is nearly equal in comparison with the case of no gravity. With increases in actuator capability, *IAR* increase a lot while *IVR* doesn't. This is because the effect of torque on the acceleraion capability increases linearly while the effect of velocity increases quadratically (Figures 8 and 9). These measures require relatively small computaions due to the compact equations.

6. CONCLUSIONS

Isotropic acceleration radius (*IAR*) and isotropic velocity radius (*IVR*) for multi-arm robots have been proposed in this paper as a local performance index of dynamic responsiveness. *IAR* can represent the acceleration capability and *IVR* can present the effects and limit of the velocity of the object. These measures make it possible to closely characterize the dynamic performance of the multi-arm robot taking account the velocity effect. An algorithm to obtain analytic expression for the measures without using pseudo-inverse has been presented.

From the results of examples, *IAR* turns out to be more effective for the multi-arm robot than the single arm robot, and what is more, *IAR* more closely represents the acceleration capability for the multi-arm robot than the dynamic manipulability does. The effect of the object velocity largely varies according to the position but that of the gravity does not. To change in actuator capability *IAR* is more sensitive than *IVR*. These measures can be used to design a manipulator to meet somes specified acceleration and velocity properties without using complex nonlinear optimization.

References

1. H. Asada, "A geometrical Representation of Manipulator Dynamics and Its Application to Arm Design" *Trans. ASME J. Dyn. Sys. Meas. Control* **105,** No. 3, 131–135 (1983).
2. T. Yoshikawa, "Manipulability of Robotic Mechanisms" *Int. J. Robotics Research* **4,** No. 2, 3–9 (1985).
3. T. Yoshikawa, "Dynamic Manipulability of Robot Manipulators" *J. Robotic System* **2,** No. 1, 113–124 (1985).
4. M. Thomas, H. C. Yuan-Chou and D. Tesar, "Optimal Actuator Sizing for Robotic Manipulators Based on Local Dynamic Criteria" *ASME J. Mech. Trans. Auto. in Design* **107,** 163–169 (June, 1985).
5. T.J. Graettinger and N.H. Krogh, "The Acceleration Radius: A Global Performance Measure for Robotic Manipulators" *IEEE J. Robotics and Automation* **4,** No. 1, 60–69 (Feb., 1988).
6. Y. Kim, "Acceleration sets of manipulators: Theory and application" *Ph.D. Thesis,* (Department of Mechanical Engineering, Carnegie Mellon University, 1989).
7. K.K. Kim and Y.S. Yoon, "Trajectory Planning of Redundant Robots by Maximizing the Moving Acceleration Radius" *Robotica* **10,** part 2, 195–203 (1992).
8. S. Lee, "Dual Redundant Arm Configuration Optimization with Task-Oriented Dual-Arm Manipulability" *IEEE Trans. Robotics and Automation* **5,** 78–97 (1989).
9. P. Chiacchio, S. Chiaverini, L. Sciavicco and B. Siciliano, "Global Task Space Manipulability Ellipsoids for Multiple-Arm Systems" *IEEE Transactions on Robotics and Automation* **7,** No. 5, 678–685 (Oct., 1991).
10. P. Chiacchio, S. Chiaverini, L. Sciavicco and B. Siciliano, "Task Space Dynamic Analysis of Multiarm System Configurations" *Int. J. Robotics Research* **10,** No. 6, 708–715 (Dec., 1991).
11. H.P. Huang, "Mathematical Formulation of Constrained Robot Systems: A Unified Approach" *Mech. Mach. Theory* **27,** No. 6, 687–700 (1992).
12. O. Khatib, "A Unified Approach for Motion and Force Control of Robot Manipulators: The Operational Space Formulation" *IEEE Journal of Robotics and Automation* **RA-3,** No. 1, 43–63 (Feb., 1987).
13. Z. Li, T.J. Tarn, and A.K. Bejczy, "Dynamic Workspace

https://doi.org/10.1017/S0263574797000362 Published online by Cambridge University Press

Analysis of Multiple Cooperating Robot Arms'' *IEEE Trans. Robotics and Automation* **7,** No. 5, 589–596 (Oct., 1991).
14. T. Yoshikawa, *Fourndaiton of Robotics: Analysis and Control* (MIT, Cambridge, Mass., 1990).
15. Y. Nakamura, Advanced Robotics: *Redundancy and Optimization* (Addison-Wesley, Reading, Mass., 1991) pp. 51–57.
16. V.C. Klema and A.J. Laub, ''The Singular Value Decomposition: Its Computation and Some Applications'' *IEEE Transaction on Automatic Control* **AC-25,** No. 2, 164–176 (April 1980).

https://doi.org/10.1017/S0263574797000362 Published online by Cambridge University Press